Published in final edited form as:
J Comp Neurol. 2006 October 20; 498(6): 810–820. doi:10.1002/cne.21089.

Distinct perisynaptic and synaptic localization of NMDA and AMPA receptors on ganglion cells in rat retina

Jun Zhang and **Jeffrey S. Diamond**
Synaptic Physiology Unit, National Institute of Neurological Disorders and Stroke, National Institutes of Health, Bethesda MD 20892-3701

Abstract

At most excitatory synapses, AMPA and NMDA receptors (AMPARs and NMDARs) occupy the postsynaptic density (PSD) and contribute to miniature excitatory postsynaptic currents (mEPSCs) elicited by single transmitter quanta. Juxtaposition of AMPARs and NMDARs may be crucial for certain types of synaptic plasticity, although extrasynaptic NMDARs also may contribute. AMPARs and NMDARs also contribute to evoked EPSCs in retinal ganglion cells (RGCs), but mEPSCs are mediated solely by AMPARs. Previous work indicates that an NMDAR component emerges in mEPSCs when glutamate uptake is reduced, suggesting that NMDARs are located near the release site but perhaps not directly beneath in the PSD. Consistent with this idea, NMDARs on RGCs encounter a lower glutamate concentration during synaptic transmission than do AMPARs. To understand better the roles of NMDARs in RGC function, we have used immunohistochemical and electron microscopic techniques to determine the precise subsynaptic localization of NMDARs in RGC dendrites. RGC dendrites were labeled retrogradely with cholera toxin B subunit (CTB) injected into the superior colliculus (SC) and identified using postembedding immunogold methods. Co-labeling with antibodies directed toward AMPARs and/or NMDARs, we found that nearly all AMPARs are located within the PSD, while most NMDARs are located perisynaptically, 100–300 nm from the PSD. This morphological evidence for exclusively perisynaptic NMDARs localizations suggests a distinct role for NMDARs in RGC function.

Keywords

NMDA; AMPA; synaptic and perisynaptic distribution; postembedding immunogold; retinal ganglion cell

INTRODUCTION

Glutamate is the major excitatory neurotransmitter in the CNS, including the retina (Slaughter and Miller, 1983; Copenhagen and Jahr, 1989; Brandstätter et al., 1998). At most mature excitatory synapses, NMDARs and AMPARs contribute to evoked and miniature EPSCs (Bekkers and Stevens, 1989; McBain and Dingledine, 1992; Silver et al., 1992, although see Clark and Cull-Candy, 2002), and immunogold electron microscopy (EM) studies indicate that NMDARs and AMPARs are colocalized in the PSD (Kharazia and Weinberg, 1997; Bernard and Bolam, 1998; Kharazia and Weinberg, 1999; Nusser, 2000). Extrasynaptic NMDARs also may participate in synaptic transmission and plasticity

Address for correspondence: Jeffrey S. Diamond, Synaptic Physiology Unit, NINDS/NIH, 35 Convent Drive, Building 35, Room 3C-1000, Bethesda, MD 20892-3701, E-mail: diamondj@ninds.nih.gov.

(Massey et al., 2004; Scimemi et al., 2004), but their localization pattern has not been analyzed by immunogold EM.

Retinal ganglion cells (RGCs) receive excitatory glutamatergic input from bipolar cells (Wässle and Boycott, 1991). Although evoked EPSCs in RGCs are mediated by AMPARs and NMDARs (Mittman et al., 1990; Diamond and Copenhagen, 1993; Lukasiewicz et al., 1997; Matsui et al., 1998; Higgs and Lukasiewicz, 1999; Matsui et al., 1999; Chen and Diamond, 2002), spontaneous mEPSCs on RGCs are mediated solely by AMPARs both in mammalian and amphibian retina (rat: Chen and Diamond, 2002; salamander: Taylor et al., 1995; newt: Matsui et al., 1998). NMDARs encounter a lower glutamate concentration during evoked EPSCs than do NMDARs and an NMDAR component emerges in mEPSCs when glutamate uptake is reduced (Chen and Diamond, 2002), suggesting that NMDARs may be located extrasynaptically on RGC dendrites (see also Matsui et al., 1998). This is in apparent contrast to pre-embedding EM studies in mammalian retina indicating that NMDAR subunits are present in postsynaptic elements at cone bipolar cell ribbon synapses (Hartveit et al., 1994; Fletcher et al., 2000; Pourcho et al., 2001). These studies did not determine the identity of the immunopositive postsynaptic process, however, and the pre-embedding immunoperoxidase method, which allows reaction product to diffuse throughout the immunopositive process, precludes distinction between localization to the PSD versus the immediately surrounding extrasynaptic membrane (Ottersen and Landsend, 1997; Nusser, 2000; Bredt and Nicoll, 2003). In the case of AMPARs, physiological and anatomical data are consistent with a synaptic localization on RGCs (Mittman et al., 1990; Taylor et al., 1995; Qin and Pourcho, 1996; Lukasiewicz et al., 1997; Qin and Pourcho, 1999; Jacoby and Wu, 2001; Chen and Diamond, 2002), although subsynaptic localization of AMPAR and the identity of immunopositive processes have not been examined with immunogold EM.

Here we examine the precise localization of NMDARs and AMPARs on dendritic membranes in rat retina with high-resolution post-embedding immunogold EM while positively identifying RGC processes with cholera toxin subunit B (CTB) retrograde tracing methods. We find that the large majority of NMDARs on RGC membranes are located at perisynaptic sites, while most AMPARs are localized to the PSD. NMDAR density is highest 100–300 nm from the edge of the PSD, suggesting that the receptors are not scattered evenly throughout the extrasynaptic membrane but are instead targeted to specific perisynaptic locations. These results indicate a novel subsynaptic localization pattern for NMDARs at a central synapse and suggest that NMDARs may play a distinct role in the integration of synaptic input by RGCs.

MATERIALS AND METHODS

CTB injection

Care and handling of animals were in accordance with NIH Animal Care and Use Committee guidelines. P15 Sprague-Dawley rats, maintained in a 12-h light/12-h dark cycle, were anesthetized with pentobarbital and immobilized in a stereotaxic. The skin over the skull was incised and small holes were drilled in the skull at sites above the right and left SCs, and 1–1.2% CTB (List Biological Lab., Campbell, CA) was injected bilaterally (2 μl each site).

Tissue fixation

5–7 d following the injection, animals were deeply anesthetized with halothane and decapitated, and both eyes were removed and hemisected. For LM immunofluorescence, eyecups then were fixed in 4% paraformaldehyde in 0.1 M phosphate buffer (PB) at pH 7.4

for 30 – 40 min at room temperature (RT). After several washes in 0.1 M phosphate-buffered saline (PBS, pH 7.4), the eyecups were cryoprotected with graded sucrose solutions at 4°C (60 min each in 15%, 20% and 30%, then overnight in 30%). The tissue was embedded in OCT compound (Tissue Tek Inc.), vertically sectioned at 14 μm on a cryostat, and collected on chrome-gelatin-coated glass slides. Whole-mounted flat retinas were prepared similarly.

For EM immunocytochemistry, retinas were isolated, immediately cut into 100–200 μm-thick strips and subjected to pH-shift fixation (Sassoe-Pognetto and Ottersen, 2000, with minor modifications). Retina strips were fixed in 4% paraformaldehyde in 0.1 M PB at pH 6.0 for 20–30 min and then in 4% paraformaldehyde plus 0.01% glutaraldehyde at pH 10.5 for 10–20 min at RT. After several washes in PB with 0.15 mM CaCl2 (pH 7.4 at 4°C), the tissue was cryoprotected with glycerol (60 min each in 10%, 20%, 30%, then overnight in 30%) in 0.1 M PB prior to freeze substitution and low-temperature embedding.

Primary antibodies

Antibodies directed toward NMDAR subunits (NR1 and NR2) and AMPAR subunits (GluR2/3 and GluR4) were purchased from Chemicon (Temecula, CA). Polyclonal anti-NR1 (Cat. No. AB1516) was raised in rabbit against a synthetic peptide (LQNQKDTVLPRRAIEREEGQLQLCSRHRES) corresponding to the C-terminus of the rat NR1 subunit and recognizes major splice variants 1a, 1b, 2a and 2b. This antibody has been characterized previously in rat retina by Western blotting (recognizing a band at ~ 116 kD) and immunocytochemistry (Fletcher et al., 2000; Gründer et al, 2000). Polyclonal anti-NR2B (Cat. No. AB1557P) was raised in rabbit against an affinity-purified C-terminal fusion protein (amino acids 984-1104). This antibody has been characterized previously in rat and cat retina by Western blotting (recognizing a band at ~ 180 kD) and immunocytochemistry (Goebel et al, 1998; Gründer et al, 2000; Pourcho et al., 2001). Polyclonal anti-GluR2/3 (Cat. No. AB1506) was raised in rabbit against an affinity-purified peptide (EGYNCYGIESVKI) from the carboxy terminus of rat GluR2 and recognizes both GluR2 and GluR3. Polyclonal anti-GluR4 (Cat. No. AB1506) was raised in rabbit against an affinity-purified peptide from the carboxy terminus (RQSSGLAVIASDLP). These two AMPAR antibodies have been widely used in mammalian retina including rat and characterized previously by Western blotting (recognizing a band at 100 ~ 110 kD) and immunocytochemistry (Ghosh et al., 2001; Grünert et al., 2002, 2003; Hack et al., 2001, 2002; Li et al., 2002). Polyclonal goat anti-CTB (List biological Lab., Campbell, CA; Cat. No. 104) has been characterized in rat retina by immunocytochemistry (Rivera and Lugo, 1998). In addition, the following antibodies have been used in studies of fish retina (Jan et al., 2001) and the CNS (Moga et al., 2003): polyclonal rabbit anti-PKC (Chemicon, to label rod bipolar cells); monoclonal mouse anti-GluR2 (Chemicon, Temecula, CA; Cat. No. MAB397), raised against a recombinant fusion protein TrpE-GluR2 (N-terminal portion, amino acids 175-430 of rat GluR2) and recognizing a band at ~ 102 kD; monoclonal mouse GluR3 (Chemicon, Temecula, CA, Cat. No. MAB5416), raised against a fusion protein (N-terminal portion, amino acids 245-451 of rat GluR3) and recognizing a band at ~ 110 kD.

LM Immunofluorescence

LM immunofluorescence was performed as described previously (Zhang et al., 2003). Slides were rinsed in PBS, blocked in 5% normal donkey serum (NDS, Sigma) in PBS for 1 hour, incubated overnight in primary antibodies (CTB diluted 1:4000, or NR1 diluted 1:30, or NR2B diluted 1:60, or GluR2/3 diluted 1:50, or GluR4 diluted 1:50) in 2% NDS plus 1% bovine serum albumin (BSA, Sigma) with 0.3% Triton X-100 at RT for anti-NMDA and at 4°C for others. After rinsing, sections were incubated for 2 hours at RT in Cy3- or FITC-conjugated donkey anti-goat IgG (1:400 & 1:100, respectively) for CTB and Cy3- or FITC-

conjugated donkey anti-rabbit IgG (1:400 & 1:100, respectively) for NR1, NR2B, GluR2/3 and GluR4. All fluorescent secondary antibodies were purchased from Jackson ImmunoResearch Laboratories (West Grove, PA). Slides were rinsed and cover-slipped with Vectashield (Vector). Whole mounted-retinas were incubated in anti-CTB for 5–7 days and the secondary antibody for one day at 4°C.

For double labeling, sections were incubated overnight in a mixture of primary antibodies (CTB 1:4000 + PKC 1:100, or CTB 1:4000 + NR1 1:30 or NR2B 1:60, or CTB 1:4000 + GluR2/3 1:50 or GluR4 1:50) in 5% NDS plus 2% BSA with 0.3% Triton X-100. Sections were rinsed and then incubated for 2 hours at RT in a mixture of two secondary antibodies (FITC-conjugated donkey anti-goat IgG and Cy3-conjugated donkey anti-rabbit IgG). Procedures for washing between and after antibody incubations were the same as for single labeling.

Specificity of immunostaining for anti-NR1, NR2B, GluR2/3 and GluR4 was confirmed with control experiments in which the antibodies were preadsorbed with the polypeptide fragments or, in the case of the NR2B antibody, the fusion protein used as the antigen (all from Chemicon: Cat. No. AG344 [NR1], Cat. No. AG262 [NR2B], Cat. No. AG305 [GluR2/3], Cat. No. AG306 [GluR4]). No fluorescence was detected with preadsorbed primary antibodies (Figure 1), or when primary antibodies were omitted in the first incubation, and no cross-reactivity between unmatched secondary antibodies was detected (data not shown).

Immunoreactivity (IR) was visualized with a confocal laser scanning microscope (Zeiss LSM-510; Thornwood, NY) through 25× and 63× oil objectives. Brightness and contrast of the final images were adjusted in Adobe Photoshop 6.0.

EM immunocytochemistry

Freeze substitution was performed as described (Petralia and Wenthold, 1999), with minor modifications. Following cryoprotection, retinal strips were plunge-frozen in liquid propane at −190°C in a Leica EM CPC (Leica, Austria). The tissue was then transferred into a freeze-substitution device (Leica EM AFS) and treated with 0.5% uranyl acetate in 100% methanol at −90°C for 36 hr, after which the temperature was increased stepwise to −45°C. Samples were washed several times in pre-cooled methanol and progressively infiltrated with Lowicryl HM20 resin (Electron Microscopy Sciences, Fort Washington, PA) (1:1 Lowicryl to methanol, 2 hr; 2:1 Lowicryl to methanol, 2 hr; 100% Lowicryl, 2 hr; 100% Lowicryl, overnight) at −45°C. Finally, the samples were polymerized (−45°C to 0°C) with ultraviolet light for 40 hours and then at RT overnight.

1 μm semi-sections were oriented to achieve optimally transverse ~70-nm-thick ultrasections, which were collected on Formvar-Carbon coated nickel-slot grids. Postembedding immunocytochemistry was performed as described (Yang et al., 2003; Zhang et al., 2004) with minor modifications. Grids were washed with distilled H_2O followed by a tris-buffered saline (TBS, 0.05 M Tris buffer, 0.7% NaCl, pH 7.6) wash, incubated in 5% BSA in TBS for 30 minutes, and then incubated in 30 μl drops of anti-goat CTB (1:3000) in TBS-Triton (TBST, 0.01% Triton X-100, pH 7.6) with 2% BSA and 0.02 M NaN_3 overnight at RT. Grids were washed on three separate drops of TBS (pH 7.6) for 10, 10, and 20 minutes, followed by TBS (pH 8.2) for 5 minutes. Grids were then incubated for 2 hours on drops of donkey anti-goat IgGs coupled to 15 or 18 nm gold particles (Electron Microscopy Sciences, Fort Washington, PA) in TBST (pH 8.2) with 2% BSA and 0.02 M NaN_3. Following washes in TBS (pH 7.6) for 5, 5 and 10 minutes, grids were washed in ultrapure water and dried. Grids were counterstained with 5% uranyl acetate and 0.3% lead citrate in distilled H_2O for 8 and 5 minutes, respectively.

In double labeling experiments, grids were incubated overnight at RT either with a mixture of anti-goat CTB (1:3000) and anti-rabbit NMDARs (NR1 1:10 and NR2B 1:30) or a mixture of CTB (1:3000) and AMPARs (GluR2/3 1:30 and GluR4 1:30), followed by a mixture of donkey anti-goat IgG (1:20) coupled to 15 or 18 nm gold particles and donkey anti-rabbit IgG (1:20) coupled to 10 nm gold particles, respectively. In triple labeling experiments, grids were first incubated with a mixture of CTB (1:3000) and NMDARs (NR1 1:10 and NR2B 1:30), followed by anti-mouse AMPARs (GluR2 1:30 and GluR3 1:30), then by a mixture of IgGs coupled to 15, 10 and 5 nm gold particles (Electron Microscopy Sciences, Fort Washington, PA), respectively. Procedures for washing and counterstaining between and after antibodies incubation were the same as for single labeling.

Specificity of immunostaining at the EM level for anti-NR1, NR2B, GluR2/3 and GluR4 was confirmed by testing antibodies that had been preadsorbed with the polypeptide fragments or fusion protein used as antigens (see description of LM methods, Figure 1). No gold labeling was seen when the secondary antibodies were applied alone, either for CTB single labeling or for double or triple labeling with NMDARs and/or AMPARs (data not shown). In addition, when one or two primary antibodies were eliminated and then the two or three appropriate secondary antibodies were applied in double or triple labelings, only gold specific for the remaining primary antibody was detected.

Grids were viewed on a JEOL 1200 EM and images were digitalized. Final figures were processed only for brightness and contrast and annotations were added in Adobe Photoshop 6.0.

Data collection

Ultrathin sections were prepared from 6 rats and sections containing IPL were chosen randomly for double labeling (CTB and NMDARs or AMPARs) and were photomontaged at 25,000× magnification. Each montage covered the full depth of the IPL, with a total area of 9892 μm^2 for NMDARs and 8959 μm^2 for AMPARs, respectively. RGC dendrites at cone bipolar dyads were analyzed when: (1) they contained retrogradely transported CTB signal, (2) related ribbon synapses were transversely cut and exhibited well-defined membranes, clefts and postsynaptic densities, (3) CTB-positive dendrites contained at least two gold particles within the PSD or more than one gold particle along the extrasynaptic plasma membrane (Baude et al., 1995; Nusser et al., 1995; Popratiloff et al., 1996; Bernard et al., 1997; Sassoe-Pognetto and Ottersen, 2000). Based on these criteria, 51 RGC dendrites for NMDARs and 48 for AMPARs were selected for quantitative analysis. In some cases, sections were triple labeled with antibodies to CTB, NMDARs and AMPARs; following the criteria above for each type of gold particle, 50 RGC dendrites, from a total area of 4233 μm^2 in three montages, were selected for analysis.

As simultaneous incubation of NMDARs and AMPARs may attenuate the signal (Racca et al., 2000), quantification of NMDAR and AMPAR expression was performed independently in double labeled tissue. CTB IR was detected only in the RGC dendritic cytoplasm, while NMDAR and AMPAR IR was detected primarily in regions near the plasma membrane.

The length of the PSD and the extrasynaptic plasma membrane of individual RGC dendrites was measured with NIH ImageJ software. Given an average thickness of 7–9 nm for the plasma membrane (Peters et al., 1991) and our criteria for transversely cut ribbon synapses, we counted gold particles within the 10 nm of the membrane as membrane-associated (see also Nusser et al., 1995). Particle density was calculated as the number of gold particles per linear micron (gold/μm). The lateral location of each gold particle was measured as the distance between the center of the particle and the middle of the PSD (for synaptic gold) or the edge of the PSD (for extrasynaptic gold).

Statistical analysis was performed using Stata 8 (Stata Corp., Texas), StatsDirect (Cheshire, UK) and Excel (Microsoft) software. Two-tailed t tests and Kolmogorov-Smirnov tests were used to compare means and distributions, respectively. Significance was concluded when $P<0.05$. Unless indicated otherwise, values are reported as mean±SEM.

RESULTS

Identification of RGC processes

To label RGCs and their dendrites, CTB was injected bilaterally into the SC, one of the two main targets of mammalian RGC axons (Siminoff et al., 1966; Bunt et al., 1974). CTB was retrogradely transported so that, at the LM level, CTB immunoreactivity was detected in the nerve fiber layer (NFL), the ganglion cell layer (GCL), the inner plexiform layer (IPL) and the inner nuclear layer (INL) in whole-mounted retinas and in transverse slices (Figure 2A–D). Numerous RGC somata of various sizes, optic nerve bundles and proximal dendrites were clearly distinguished (Figure 2A, D), similar to reports in ground squirrel showing that three different sizes of ganglion cells were retrogradely labeled when CTB was injected bilaterally into the SC (Rivera & Lugo. 1998). In samples of 22 whole-mounted retinas, the average density of labeled RGCs was 3214 ± 685 cells/mm^2, comparable to previous measures obtained with other retrograde tracers in rat retina (2116–2725 cells/mm^2: Linden and Perry, 1983; Villegas-Perez et al., 1988; Vecino et al., 2002) that labeled ~90% of the ganglion cell population (Linden and Perry, 1983). The primary dendrites of CTB-labeled RGC clearly extended into the IPL and their higher-order branches and distal dendrites formed two bands in the IPL (Figure 2B, D). At higher magnification, two distinct bands were evident in the outer and middle thirds of the IPL, which may correspond to regions of input from OFF and ON cone bipolar terminals, respectively (Nelson et al., 1978; Peichl and Wässle, 1981; Amthor et al., 1989), whereas rod bipolar terminals, labeled with antibodies to PKC (Kosaka et al., 1998), occupied the inner third (Figure 2F). This morphological view of IPL sublaminae, in which the division between sublamina a and b occurs at the outer third of the IPL, is similar to that described in cat (Nelson et al., 1978; Peichl and Wässle, 1981) but contrasts slightly with physiological experiments in rat suggesting that the a-b border occurs in the middle of the IPL (Euler et al., 1996). Additionally, a relatively small number of CTB-positive “displaced” RGCs appeared in the INL (Figure 2C, E; Bunt et al., 1974; Buhl and Dann, 1988).

At the ultrastructural level, gold particles labeling CTB were present in the perikarya and proximal and distal dendrites of RGCs but were absent from the nucleus (Figure 2G, H). CTB-positive RGC dendrites were found in sublamina a and b of the IPL and rarely constituted more than one of the two postsynaptic elements in the dyad synapse (Figure 2I, J). The mean density of CTB-associated gold particles in RGC dendrites (15.45±2.97 gold/μm^2; n=37) was 59 times higher than that in Müller cell processes (0.26±0.04 gold/μm^2; n=35; $P<0.001$), indicating that CTB gold labeling was specific to RGC processes.

NMDARs on RGCs are distributed perisynaptically

NMDARs were labeled with antibodies recognizing NR1 and NR2B subunits (Takumi 1999). IR at the LM level was similar to previous reports in rat retina (Fletcher et al., 2000; Kalloniatis et al., 2004). Intense, punctate labeling was evident in the IPL and OPL, in addition to somatic labeling in the GCL and INL (Figure 3A, C). Double labeling of NR1 or NR2B and CTB showed that all CTB-positive RGCs were NR1- or NR2B- positive (Figure 3B, D). Not all NR1 or NR2B immunopositive puncta were colocalized with CTB labeled ganglion cell dendrites, however, indicating that NMDARs also are expressed in other cell types. NR1 and NR2B IR also was evident in the outer plexiform layer.

At the EM level, antibodies toward NR1 and NR2B were combined (Nusser et al., 1998; Petralia et al., 1999; Petralia and Wenthold, 1999; Takumi et al., 1999; Racca et al., 2000) and applied to tissue that had been retrogradely labeled with CTB. The large majority (97%) of NMDAR-immunogold particles was located outside the PSD, distributed primarily along the extrasynaptic plasma membrane (Figure 3E, F, 5A). Similar patterns were observed in sublamina a and b of the IPL (Figure 3E, F); the density of gold particles in the two sublaminae were not significantly different (2.91 ± 0.41 [n=24] vs. 3.54 ± 0.23 [n=27], P>0.1). Immunogold particles were detected mostly on the intracellular surface of the extrasynaptic plasma membrane; some particles were present in the postsynaptic cytoplasm of RGC dendrites and somata (data not shown), consistent with LM results (Figure 3A–D). In the single instance in which both postsynaptic elements at the dyad were CTB-positive RGC processes, both expressed NMDARs perisynaptically (data not shown). In 51 identified RGC dendrites at cone dyad, 92% (47) expressed NMDARs perisynaptically and 8% (4) exhibited both synaptic and extrasynaptic expression. 80% of the other CTB-negative postsynaptic process (presumable amacrine cells) were immunonegative (Figure 3F), consistent with previous reports (Fletcher et al., 2000; Pourcho et al., 2001).

The tangential distribution of NMDAR gold particles was analyzed within and outside the synapse. Particles within the synapse were located in the lateral margin of the PSD but were not seen in the middle (Figure 5B). Extrasynaptically, 76% of the gold particles were located within 480 nm of the PSD edge (Figure 5A).

The mean length of the extrasynaptic plasma membrane of RGC dendritic profiles (1592±96 nm, n = 51) was much greater than that of the PSD (180±8 nm, n = 51), which would favor detection of extrasynaptic receptors. However, the mean density of extrasynaptic NMDAR gold particles (2.98±0.24 per μm) was almost four times greater than that in the PSD (0.77±0.38 per μm, $P < 0.0001$; Table 1). To compare density in the PSD and at varying distances from the synapse, the distance along the membrane between each membrane-associated extrasynaptic particle and the edge of the PSD was measured and collected into 180 nm bins (Figure 5C). Extrasynaptic NMDAR density within 720 nm of the edge of the synapse was 3–11 times higher than in the PSD (Figure 5C, $P < 0.001$). Immunopositive processes usually contained numerous perisynaptic gold particles (Figure 5D), enhancing the precision of density calculations.

AMPARs on RGCs are localized primarily within the PSD

AMPARs were labeled with antibodies recognizing the GluR2/3 and GluR4 subunits (Takumi et al., 1999). IR at the LM level was evident primarily in the OPL and IPL; GluR4 signal in the IPL segregated clearly into two distinct bands, but no such stratification was observed with GluR2/3 (Figure 4A, B, C, D), similar to previous studies in rat retina (Peng et al., 1995; Hack et al., 2002). These antibodies were combined to enhance the signal for EM immunocytochemistry. At the EM level, 77% of AMPAR immunogold particles in RGC dendritic profiles were located within the PSD (Figure 4E, F, 5E). A consistent postsynaptic labeling pattern was observed throughout the IPL, and the density of AMPAR immunogold was not significantly different in sublamina a and b (25.35 ± 5.89 [n=21] vs. 26.67 ± 8.87 [n=22], $P > 0.5$). 23% of AMPAR immunogold was associated with the extrasynaptic plasma membrane (Figure 4F) or in the RGC dendritic cytoplasm. 43 of 48 identified RGC dendrites (90%) expressed AMPARs synaptically; the remaining profiles had no gold in the PSD but exhibited IR either extrasynaptically or in the cytoplasm. Generally, when the postsynaptic RGC profile was AMPAR-positive, the other postsynaptic process in the dyad was negative (Figure 4E, F), consistent with previous reports (Qin and Pourcho, 1996, 1999; Brandstätter, 2002).

The tangential distribution of gold particles within the synapse indicated that AMPA-IR was directed toward the center of the PSD (Figure 5F). Gold particles at extrasynaptic membranes were observed only rarely (Figure 5E). The mean length of the PSD for AMPAR-positive RGC dendrites was 181±9 nm (n = 43), nearly identical to the PSDs in NMDAR-positive RGC dendritic profiles. The mean particle density of AMPARs in the postsynaptic membrane (15.8±1.8 gold/μm^2) was significantly greater than that in extrasynaptic membrane (0.55±0.15 gold/μm^2, $P < 0.0001$; Table 1). AMPAR immunogold density within the PSD was 7–66 times higher than in the perisynaptic membrane (Figure 5G).

Simultaneous labeling of NMDARs and AMPARs in CTB-positive RGCs

In a subset of experiments, tissue was triple-labeled for CTB, AMPARs and NMDARs. Of 50 identified RGC dendrites at cone dyads, 40 (80%) were simultaneously positive for synaptic AMPARs and extrasynaptic NMDARs (Figure 6A, B), 5 (10%) were AMPAR-negative synaptically but NMDAR-positive extrasynaptically, and 5 (10%) were NMDAR-positive synaptically. Three of the 5 profiles in this last group were AMPAR-positive synaptically (Figure 6C), indicating that NMDARs and AMPARs are colocalized in the PSD of only a very small fraction (6%) of RGC dendrites.

DISCUSSION

The results presented here demonstrate strikingly different subsynaptic localization patterns of AMPARs and NMDARs on RGC dendrites in rat retina. Most AMPARs are located within the PSD, similar to most central synapses, but nearly all NMDARs are located extrasynaptically. NMDARs are not merely scattered evenly throughout the extrasynaptic membrane, however; rather, they are located primarily 100–300 nm from the edge of the PSD, suggesting that they are anchored at specific locations by submembrane receptor scaffolding proteins in RGC dendrites. The contrasting localization patterns of NMDARs and AMPARs do not reflect distinct synapse populations, because they appear at individual synapses that are immunopositive for both receptor types. Moreover, similar patterns occur in sublaminae a and b of the IPL, indicating that synapses onto ON and OFF RGCs express AMPARs synaptically and NMDARs perisynaptically.

Methodological considerations

A range of different fixation methods and times were tested in an effort to strike an optimal balance between ultrastructural integrity and antigenicity. Gentle fixation and short incubation times were necessary, because NMDA receptor antigenicity decreases markedly with strong, prolonged fixation (Fletcher et al., 2000). In our hands, existing fixation protocols used for post-embedding NMDAR EM (Petralia and Wenthold 1999; Petralia et al., 1999), when applied to retina, yielded undetectable NMDAR IR, although tissue preservation was improved relative to that shown here.

Most functional NMDARs comprise two NR1 and two NR2 subunits (Dingledine 1999); many functional properties and targeting characteristics appear to be determined by the specific complement of NR2 (A–D) subunits (Cull-Candy & Leszkiewicz 2004). For example, extrasynaptic NMDARs contain primarily the NR2B subunit, while NR2A-containing receptors are located primarily in the PSD (Tovar & Westbrook 1999; Hartveit et al., 1994). Preliminary data indicates that NR2B-containing receptors contribute to light-evoked EPSCs (T. Kalbaugh and S. Chen, unpublished), prompting us to use a cocktail of NR1 and NR2B antibodies. Antibodies to both subunits intensely stained the IPL and co-localized with CTB IR (Figure 3B, 3D), suggesting that the NR1 and NR2B antibodies labeled RGC NMDARs with similar efficacy. Preliminary data indicates a similar, primarily

perisynaptic pattern of NMDAR expression (though less intense labeling) when the NR1 antibody is used alone (Zhang and Diamond, unpublished). It remains possible, however, that the small fraction (3%) of NMDARs in the postsynaptic density reflects NR2A-containing receptors, as suggested previously (Hartveit et al., 1994). Although immunofluroscent puncta for NR2A and NR2B subunits have been shown to be clustered at different synaptic "hot spots" in the IPL (Fletcher et al., 2000), further ultrastructural studies are required to determine the specific subsynaptic distribution of different NR2 subunits (NR2A-D) in RGC dendrites.

Perisynaptic location of NMDARs limits their activation during quantal events

The perisynaptic distribution of NMDARs observed here contributes strong morphological support to physiological evidence that NMDARs on RGC dendrites are located a greater distance from the release site than are AMPARs. NMDARs are not activated by glutamate released from a single vesicle (Taylor et al., 1995; Matsui et al., 1998; Chen and Diamond, 2002), unless glutamate uptake is reduced (Chen and Diamond, 2002), and NMDARs encounter a lower synaptic glutamate concentration during evoked responses than do AMPARs (Chen and Diamond, 2002). Taken together, these previous physiological data and the morphological results presented here suggest that transmitter released from a single vesicle is not sufficient to activate NMDARs located perisynaptically, several hundred nm from the release site. The transmitter concentration reaching the NMDARs appears to be diminished by dilution into the larger volume of the perisynaptic space and by rapid removal of free transmitter by glutamate transporters. During an evoked response, however, NMDARs are activated more easily by higher levels of transmitter, presumably generated by multivesicular release from individual ribbon synapses (Singer et al., 2004) and/or glutamate spillover between synapses.

Glutamate transporters buffer synaptically released glutamate on a very rapid time scale (Diamond and Jahr, 1997; Diamond, 2005), but during a synaptic event extrasynaptic glial transporters affect only slightly the glutamate concentration waveform within the synaptic cleft (Diamond and Jahr, 1997). The large effect of uptake on NMDAR activation at RGC synapses (Chen and Diamond, 2002), then, indicates a different arrangement at the synapses studied here, one in which transporters may be positioned between the release site and the NMDARs and therefore able to intercept a considerable fraction of synaptically released glutamate before it reaches the receptors. The density of NMDARs peaks at about 200 nm from the edge of the PSD (Figure 5A); transporters could, therefore, limit NMDAR activation if they were located within the synaptic cleft (i.e., the PSD or the apposed presynaptic membrane) or in the immediately perisynaptic region. As this area appears to contain only neuronal pre- and postsynaptic membranes, it seems likely that neuronal glutamate transporters limit the activation of perisynaptic NMDARs. The subsynaptic localization of glutamate transporters and the specific transporter subtype(s) acting at these synapses remains to be determined.

AMPARs are located within the PSD

The results presented here demonstrate that AMPARs are localized predominantly within the PSD, consistent with physiological evidence that they mediate synaptic activation of RGCs (Lukasiewicz et al., 1997; Jacoby and Wu, 2001; Chen and Diamond, 2002). Moreover, AMPARs are expressed at the highest density in the middle of the PSD (Figure 4, 5F), ensuring their rapid activation by synaptically released glutamate and, perhaps, minimizing molecular interactions with perisynaptic NMDARs and associated proteins. Perisynaptic AMPARs were observed only very rarely (Figure 4F,5E) and may have reflected receptors in transit to or from the synaptic cleft (Bredt and Nicoll, 2003). The nearly complete spatial segregation of AMPARs and NMDARs suggests that any synaptic

plasticity in RGC dendrites (Hosoya et al., 2005) may be distinct from NMDAR-dependent forms of plasticity studied elsewhere in the brain (Malenka and Bear, 2004).

Receptor localization is similar at synapses onto ON and OFF RGCs

ON and OFF RGCs play apparently inverse processing roles in the retinal network and receive synaptic input in distinct layers of the IPL. Morphological and molecular differences in synapses onto ON and OFF RGCs, however, have not been reported. Both RGC types receive excitatory input mediated by NMDARs and AMPARs (Mittman et al., 1990; Cohen et al., 1994), and ON and OFF parasol RGCs in primate retina express glutamate receptors at similar densities (Lin et al., 2002). At the immunogold EM level, we observed no significant difference in the subsynaptic localization patterns and densities of either AMPARs or NMDARs in the ON and OFF sublaminae of the IPL. It remains to be investigated whether receptors in ON and OFF RGCs comprise distinct subunit combinations that may underlie different synaptic processing tasks (e.g., Duprat et al., 2003; Perez-Otano and Ehlers, 2004).

Comparison with previous work

The punctate pattern of NMDAR antibody labeling observed here at the LM level (Figure 3) is similar to that reported previously (Hartveit et al., 1994;Fletcher et al., 2000;Pourcho et al., 2001), but our finding that NMDARs are largely excluded from the PSD in RGC dendrites contradicts previous pre-embedding EM studies (Hartveit et al., 1994;Pourcho et al., 2001). The discrepancies between our and previous results are likely due to methodological differences. First, pre-embedding immunoperoxidase methods (Hartveit et al., 1994;Fletcher et al., 2000;Pourcho et al., 2001) offer significantly greater sensitivity, albeit with less spatial resolution, than the post-embedding immunogold technique used here. The peroxidase reaction product can diffuse within the immunopositive process and may bind non-specifically to structures in the PSD (Baude et al., 1995;Ottersen et al., 1998), making it difficult to determine quantitatively the precise subsynaptic localization of receptors (Ottersen and Landsend, 1997). The post-embedding immunogold method reduces such artifacts because antibodies are applied directly to the surface of thin sections and the resin restricts label diffusion, permitting higher spatial resolution (Ottersen and Landsend, 1997;Nusser et al., 1998;Takumi et al., 1999;Nusser, 2000). Consequently, significant differences between pre- and post-embedding approaches have been observed in the retina (Haverkamp et al., 2001) and elsewhere in the CNS (Baude et al., 1993;Nusser et al., 1994;Baude et al., 1995;Bernard et al., 1997;Bernard and Bolam, 1998). Second, in previous studies of synaptic glutamate receptor localization in the IPL (Hartveit et al., 1994;Qin and Pourcho, 1996,1999;Fletcher et al., 2000;Pourcho et al., 2001;Hack et al., 2002), the specific cellular identity of the immunopositive postsynaptic processes was not positively determined. NMDAR-immunopositive processes, therefore, may have belonged to amacrine cells, a subset of which receive synaptic inputs mediated by NMDARs (Dixon and Copenhagen, 1992;Goebel et al., 1998;Fletcher et al., 2000;Gründer et al., 2000). Here, retrograde labeling of RGCs by CTB provided a reliable marker of RGC process in the IPL (Figure 2), enabling receptor localization to be examined on identified RGC processes.

Molecular mechanisms underlying perisynaptic NMDAR localization

At most excitatory synapses in the brain, glutamate receptors and associated signaling proteins are organized in the postsynaptic membrane by a family of membrane-associated guanylate kinases (MAGUKs) characterized by PDZ interaction domains (Kim and Sheng, 2004). Although NMDARs are most often associated with PSD-95 (Kennedy, 1997), the two proteins exhibit distinct developmental profiles (Sans et al., 2000) and NMDARs cluster in the absence of PSD-95 (Migaud et al., 1998), suggesting that other MAGUKs also may anchor NMDARs in the membrane. In the hippocampus another MAGUK, SAP-102, is

expressed early in development (Sans et al., 2000), when many NMDARs are extrasynaptic (Perez-Otano and Ehlers, 2004), making it an attractive candidate for anchoring perisynaptic NMDARs in RGCs. Immunofluorescence microscopy reveals punctate expression of PSD-93, PSD-95 and SAP-102 in the IPL of rat retina (Koulen et al., 1998; Koulen, 1999; Fletcher et al., 2000), although perisynaptic co-localization of NMDARs and specific MAGUKs remains to be determined.

Acknowledgments

We thank Drs. Pierre Brown and Charles Gerfen for performing CTB injections; Drs. Brian Andrews, Christine Winters, Natalia Pivovarova and Christine Brantner for help with freeze-substitution; the NINDS LM and EM facilities for technical advice and assistance; and Drs. Brian Andrews, Susan Cheng and Ron Petralia for comments on the manuscript.

This work was supported by the National Institute of Neurological Disorders and Stroke Intramural Research Program.

LITERATURE CITED

Amthor FR, Takahashi ES, Oyster CW. Morphologies of rabbit retinal ganglion cells with complex receptive fields. J Comp Neurol. 1989; 280:97–121. [PubMed: 2918098]

Baude A, Nusser Z, Molnar E, McIlhinney RA, Somogyi P. High-resolution immunogold localization of AMPA type glutamate receptor subunits at synaptic and non-synaptic sites in rat hippocampus. Neuroscience. 1995; 69:1031–1055. [PubMed: 8848093]

Baude A, Nusser Z, Roberts JD, Mulvihill E, McIlhinney RA, Somogyi P. The metabotropic glutamate receptor (mGluR1 alpha) is concentrated at perisynaptic membrane of neuronal subpopulations as detected by immunogold reaction. Neuron. 1993; 11:771–787. [PubMed: 8104433]

Bekkers JM, Stevens CF. NMDA and non-NMDA receptors are co-localized at individual excitatory synapses in cultured rat hippocampus. Nature. 1989; 341:230–233. [PubMed: 2571090]

Bernard V, Bolam JP. Subcellular and subsynaptic distribution of the NR1 subunit of the NMDA receptor in the neostriatum and globus pallidus of the rat: co-localization at synapses with the GluR2/3 subunit of the AMPA receptor. Eur J Neurosci. 1998; 10:3721–3736. [PubMed: 9875351]

Bernard V, Somogyi P, Bolam JP. Cellular, subcellular, and subsynaptic distribution of AMPA-type glutamate receptor subunits in the neostriatum of the rat. J Neurosci. 1997; 17:819–833. [PubMed: 8987803]

Brandstätter JH. Glutamate receptors in the retina: the molecular substrate for visual signal processing. Curr Eye Res. 2002; 25:327–331. [PubMed: 12789538]

Brandstätter JH, Koulen P, Wassle H. Diversity of glutamate receptors in the mammalian retina. Vision Res. 1998; 38:1385–1397. [PubMed: 9667006]

Bredt DS, Nicoll RA. AMPA receptor trafficking at excitatory synapses. Neuron. 2003; 40:361–379. [PubMed: 14556714]

Buhl EH, Dann JF. Morphological diversity of displaced retinal ganglion cells in the rat: a lucifer yellow study. J Comp Neurol. 1988; 269:210–218. [PubMed: 3356810]

Bunt AH, Lund RD, Lund JS. Retrograde axonal transport of horseradish peroxidase by ganglion cells of the albino rat retina. Brain Res. 1974; 73:215–228. [PubMed: 4133900]

Chen S, Diamond JS. Synaptically released glutamate activates extrasynaptic NMDA receptors on cells in the ganglion cell layer of rat retina. J Neurosci. 2002; 22:2165–2173. [PubMed: 11896156]

Clark BA, Cull-Candy SG. Activity-dependent recruitment of extrasynaptic NMDA receptor activation at an AMPA receptor-only synapse. J Neurosci. 2002; 22:4428–4436. [PubMed: 12040050]

Cohen ED, Zhou ZJ, Fain GL. Ligand-gated currents of alpha and beta ganglion cells in the cat retinal slice. J Neurophysiol. 1994; 72:1260–1269. [PubMed: 7528793]

Copenhagen DR, Jahr CE. Release of endogenous excitatory amino acids from turtle photoreceptors. Nature. 1989; 341:536–539. [PubMed: 2477707]

Diamond JS. Deriving the glutamate clearance time course from transporter currents in CA1 hippocampal astrocytes: transmitter uptake gets faster during development. J Neurosci. 2005; 25:2906–2916. [PubMed: 15772350]

Cull-Candy SC, Leszkiewicz DN. Role of distinct NMDA receptor subtypes at central synapses. Sci STKE. 2004; 2004:255.

Diamond JS, Copenhagen DR. The contribution of NMDA and non-NMDA receptors to the light-evoked input-output characteristics of retinal ganglion cells. Neuron. 1993; 11:725–738. [PubMed: 8104431]

Diamond JS, Jahr CE. Transporters buffer synaptically released glutamate on a submillisecond time scale. J Neurosci. 1997; 17:4672–4687. [PubMed: 9169528]

Dingledine R, Borges K, Bowie D, Traynelis SF. The glutamate receptor ion channels. Pharmacol Rev. 1999; 51(1):7–61. [PubMed: 10049997]

Dixon DB, Copenhagen DR. Two types of glutamate receptors differentially excite amacrine cells in the tiger salamander retina. J Physiol. 1992; 449:589–606. [PubMed: 1355793]

Duprat F, Daw M, Lim W, Collingridge G, Isaac J. GluR2 protein-protein interactions and the regulation of AMPA receptors during synaptic plasticity. Philos Trans R Soc Lond B Biol Sci. 2003; 358:715–720. [PubMed: 12740117]

Euler T, Schneider H, Wässle H. Glutamate responses of bipolar cells in a slice preparation of the rat retina. J Neurosci. 1996; 16:2934–2944. [PubMed: 8622124]

Fletcher EL, Hack I, Brandstätter JH, Wässle H. Synaptic localization of NMDA receptor subunits in the rat retina. J Comp Neurol. 2000; 420:98–112. [PubMed: 10745222]

Ghosh KK, Haverkamp S, Wässle H. Glutamate receptors in the rod pathway of the mammalian retina. J Neurosci. 2001; 21:8636–8647. [PubMed: 11606651]

Goebel DJ, Aurelia JL, Tai Q, Jojich L, Poosch MS. Immunocytochemical localization of the NMDA-R2A receptor subunit in the cat retina. Brain Res. 1998; 808:141–154. [PubMed: 9767152]

Gründer T, Kohler K, Kaletta A, Guenther E. The distribution and developmental regulation of NMDA receptor subunit proteins in the outer and inner retina of the rat. J Neurobiol. 2000; 44:333–342. [PubMed: 10942886]

Grünert U, Haverkamp S, Fletcher EL, Wässle H. Synaptic distribution of ionotropic glutamate receptors in the inner plexiform layer of the primate retina. J Comp Neurol. 2002; 447:138–151. [PubMed: 11977117]

Grünert U, Lin B, Martin PR. Glutamate receptors at bipolar synapses in the inner plexiform layer of the primate retina: light microscopic analysis. J Comp Neurol. 2003; 466:136–147. [PubMed: 14515245]

Hack I, Frech M, Peichl L, Brandstätter JH. Heterogeneous distribution of AMPA glutamate receptor subunits at the photoreceptor synapses of rodent retina. Eur J Neurosci. 2001; 13:15–24. [PubMed: 11135000]

Hack I, Koulen P, Peichl L, Brandstätter JH. Development of glutamatergic synapses in the rat retina: the postnatal expression of ionotropic glutamate receptor subunits. Vis Neurosci. 2002; 19:1–13. [PubMed: 12180854]

Hartveit E, Brandstätter JH, Sassoe-Pognetto M, Laurie DJ, Seeburg PH, Wässle H. Localization and developmental expression of the NMDA receptor subunit NR2A in the mammalian retina. J Comp Neurol. 1994; 348:570–582. [PubMed: 7836563]

Haverkamp S, Grünert U, Wässle H. The synaptic architecture of AMPA receptors at the cone pedicle of the primate retina. J Neurosci. 2001; 21:2488–2500. [PubMed: 11264323]

Higgs MH, Lukasiewicz PD. Glutamate uptake limits synaptic excitation of retinal ganglion cells. J Neurosci. 1999; 19:3691–3700. [PubMed: 10234001]

Hosoya T, Baccus SA, Meister M. Dynamic predictive coding by the retina. Nature. 2005; 436:71–77. [PubMed: 16001064]

Jacoby RA, Wu SM. AMPA-preferring receptors mediate excitatory non-NMDA responses of primate retinal ganglion cells. Vis Neurosci. 2001; 18:703–710. [PubMed: 11925006]

Jan K, Studholme KE, Yazulla S. Localization of the AMPA subunit GluR2 in the outer plexiform layer of goldfish retina. J Comp Neurol. 2001; 441:155–167. [PubMed: 11745642]

Kalloniatis M, Sun D, Foster L, Haverkamp S, Wässle H. Localization of NMDA receptor subunits and mapping NMDA drive within the mammalian retina. Vis Neurosci. 2004; 21:587–597. [PubMed: 15595182]

Kennedy MB. The postsynaptic density at glutamatergic synapses. Trends Neurosci. 1997; 20:264–268. [PubMed: 9185308]

Kharazia VN, Weinberg RJ. Tangential synaptic distribution of NMDA and AMPA receptors in rat neocortex. Neurosci Lett. 1997; 238:41–44. [PubMed: 9464650]

Kharazia VN, Weinberg RJ. Immunogold localization of AMPA and NMDA receptors in somatic sensory cortex of albino rat. J Comp Neurol. 1999; 412:292–302. [PubMed: 10441757]

Kim E, Sheng M. PDZ domain proteins of synapses. Nat Rev Neurosci. 2004; 5:771–781. [PubMed: 15378037]

Kosaka J, Suzuki A, Morii E, Nomura S. Differential localization and expression of alpha and beta isoenzymes of protein kinase C in the rat retina. J Neurosci Res. 1998; 54:655–663. [PubMed: 9843156]

Koulen P, Fletcher EL, Craven SE, Bredt ES, Wässle H. Immunocytochemical localization of postsynaptic density protein PSD-95 in the mammalian retina. J Neurosci. 1998; 18:10136–10149. [PubMed: 9822767]

Koulen P. Localization of synapse-associated proteins during postnatal development of the rat retina. Eur J Neurosci. 1999; 11:2007–2018. [PubMed: 10336670]

Li W, Trexler B, Massey S. Glutamate receptors at rod bipolar ribbon synapses in the rabbit retina. J Comp Neurol. 2002; 448:230–248. [PubMed: 12115706]

Lin B, Martin PR, Grünert U. Expression and distribution of ionotropic glutamate receptor subunits on parasol ganglion cells in the primate retina. Vis Neurosci. 2002; 19:453–465. [PubMed: 12511078]

Linden R, Perry VH. Massive retinotectal projection in rats. Brain Res. 1983; 272:145–149. [PubMed: 6616190]

Lukasiewicz PD, Wilson JA, Lawrence JE. AMPA-preferring receptors mediate excitatory synaptic inputs to retinal ganglion cells. J Neurophysiol. 1997; 77:57–64. [PubMed: 9120596]

Malenka RC, Bear MF. LTP and LTD: an embarrassment of riches. Neuron. 2004; 44:5–21. [PubMed: 15450156]

Massey PV, Johnson BE, Moult PR, Auberson YP, Brown MW, Molnar E, Collingridge GL, Bashir ZI. Differential roles of NR2A and NR2B-containing NMDA receptors in cortical long-term potentiation and long-term depression. J Neurosci. 2004; 24:7821–7828. [PubMed: 15356193]

Matsui K, Hosoi N, Tachibana M. Excitatory synaptic transmission in the inner retina: paired recordings of bipolar cells and neurons of the ganglion cell layer. J Neurosci. 1998; 18:4500–4510. [PubMed: 9614227]

Matsui K, Hosoi N, Tachibana M. Active role of glutamate uptake in the synaptic transmission from retinal nonspiking neurons. J Neurosci. 1999; 19:6755–6766. [PubMed: 10436033]

McBain C, Dingledine R. Dual-component miniature excitatory synaptic currents in rat hippocampal CA3 pyramidal neurons. J Neurophysiol. 1992; 68:16–27. [PubMed: 1355525]

Migaud M, Charlesworth P, Dempster M, Webster LC, Watabe AM, Makhinson M, He Y, Ramsay MF, Morris RG, Morrison JH, O'Dell TJ, Grant SG. Enhanced long-term potentiation and impaired learning in mice with mutant postsynaptic density-95 protein. Nature. 1998; 396:433–439. [PubMed: 9853749]

Mittman S, Taylor WR, Copenhagen DR. Concomitant activation of two types of glutamate receptor mediates excitation of salamander retinal ganglion cells. J Physiol. 1990; 428:175–197. [PubMed: 2172521]

Moga DE, Janssen WG, Vissavajjhala P, Czelusniak SM, Moran TM, Hof PR, Morrison JH. Glutamate receptor subunit 3 (GluR3) immunoreactivity delineates a subpopulation of parvalbumin-containing interneurons in the rat hippocampus. J Comp Neurol. 2003; 462:15–28. [PubMed: 12761821]

Nelson R, Famiglietti EV Jr, Kolb H. Intracellular staining reveals different levels of stratification for on- and off-center ganglion cells in cat retina. J Neurophysiol. 1978; 41:472–483. [PubMed: 650277]

Nusser Z. AMPA and NMDA receptors: similarities and differences in their synaptic distribution. Curr Opin Neurobiol. 2000; 10:337–341. [PubMed: 10851167]

Nusser Z, Mulvihill E, Streit P, Somogyi P. Subsynaptic segregation of metabotropic and ionotropic glutamate receptors as revealed by immunogold localization. Neuroscience. 1994; 61:421–427. [PubMed: 7969918]

Nusser Z, Roberts JD, Baude A, Richards JG, Somogyi P. Relative densities of synaptic and extrasynaptic GABAA receptors on cerebellar granule cells as determined by a quantitative immunogold method. J Neurosci. 1995; 15:2948–2960. [PubMed: 7722639]

Nusser Z, Lujan R, Laube G, Roberts JD, Molnar E, Somogyi P. Cell type and pathway dependence of synaptic AMPA receptor number and variability in the hippocampus. Neuron. 1998; 21:545–559. [PubMed: 9768841]

Ottersen OP, Landsend AS. Organization of glutamate receptors at the synapse. Eur J Neurosci. 1997; 9:2219–2224. [PubMed: 9464917]

Ottersen OP, Takumi Y, Matsubara A, Landsend AS, Laake JH, Usami S. Molecular organization of a type of peripheral glutamate synapse: the afferent synapses of hair cells in the inner ear. Prog Neurobiol. 1998; 54:127–148. [PubMed: 9481795]

Peichl L, Wässle H. Morphological identification of on- and off-centre brisk transient (Y) cells in the cat retina. Proc R Soc Lond B Biol Sci. 1981; 212:139–153. [PubMed: 6166011]

Peng YW, Blackstone CD, Huganir RL, Yau KW. Distribution of glutamate receptor subtypes in the vertebrate retina. Neuroscience. 1995; 66:483–497. [PubMed: 7477889]

Perez-Otano I, Ehlers MD. Learning from NMDA receptor trafficking: clues to the development and maturation of glutamatergic synapses. Neurosignals. 2004; 13:175–189. [PubMed: 15148446]

Peters, A.; Palay, S.; Webster, H. The fine structure of the nervous system: neurons and their supporting cells. 3. New York: Oxford University Press; 1991.

Petralia, RS.; Wenthold, RJ. Immunocytochemistry of NMDA receptors. Totowa, NJ: Humana Press; 1999.

Petralia RS, Esteban JA, Wang YX, Partridge JG, Zhao HM, Wenthold RJ, Malinow R. Selective acquisition of AMPA receptors over postnatal development suggests a molecular basis for silent synapses. Nat Neurosci. 1999; 2:31–36. [PubMed: 10195177]

Popratiloff A, Weinberg RJ, Rustioni A. AMPA receptor subunits underlying terminals of fine-caliber primary afferent fibers. J Neurosci. 1996; 16:3363–3372. [PubMed: 8627372]

Pourcho RG, Qin P, Goebel DJ. Cellular and subcellular distribution of NMDA receptor subunit NR2B in the retina. J Comp Neurol. 2001; 433:75–85. [PubMed: 11283950]

Qin P, Pourcho RG. Distribution of AMPA-selective glutamate receptor subunits in the cat retina. Brain Res. 1996; 710:303–307. [PubMed: 8963676]

Qin P, Pourcho RG. Localization of AMPA-selective glutamate receptor subunits in the cat retina: a light- and electron-microscopic study. Vis Neurosci. 1999; 16:169–177. [PubMed: 10022488]

Racca C, Stephenson FA, Streit P, Roberts JD, Somogyi P. NMDA receptor content of synapses in stratum radiatum of the hippocampal CA1 area. J Neurosci. 2000; 20:2512–2522. [PubMed: 10729331]

Rivera N, Lugo N. Four retinal ganglion cell types that project to the superior colliculus in the thirteen-lined ground squirrel (Spermophilus tridecemlineatus). J Comp Neurol. 1998; 396:105–120. [PubMed: 9623890]

Sans N, Petralia RS, Wang YX, Blahos J 2nd, Hell JW, Wenthold RJ. A developmental change in NMDA receptor-associated proteins at hippocampal synapses. J Neurosci. 2000; 20:1260–1271. [PubMed: 10648730]

Sassoe-Pognetto M, Ottersen OP. Organization of ionotropic glutamate receptors at dendrodendritic synapses in the rat olfactory bulb. J Neurosci. 2000; 20:2192–2201. [PubMed: 10704494]

Scimemi A, Fine A, Kullmann DM, Rusakov DA. NR2B-containing receptors mediate cross talk among hippocampal synapses. J Neurosci. 2004; 24:4767–4777. [PubMed: 15152037]

Silver RA, Traynelis SF, Cull-Candy SG. Rapid-time-course miniature and evoked excitatory currents at cerebellar synapses in situ. Nature. 1992; 355:163–166. [PubMed: 1370344]

Siminoff R, Schwassmann HO, Kruger L. An electrophysiological study of the visual projection to the superior colliculus of the rat. J Comp Neurol. 1966; 127:435–444. [PubMed: 5968989]

Singer JH, Lassova L, Vardi N, Diamond JS. Coordinated multivesicular release at a mammalian ribbon synapse. Nat Neurosci. 2004; 7:826–833. [PubMed: 15235608]

Slaughter MM, Miller RF. The role of excitatory amino acid transmitters in the mudpuppy retina: an analysis with kainic acid and N-methyl aspartate. J Neurosci. 1983; 3:1701–1711. [PubMed: 6135763]

Takumi Y, Ramirez-Leon V, Laake P, Rinvik E, Ottersen OP. Different modes of expression of AMPA and NMDA receptors in hippocampal synapses. Nat Neurosci. 1999; 2:618–624. [PubMed: 10409387]

Taylor WR, Chen E, Copenhagen DR. Characterization of spontaneous excitatory synaptic currents in salamander retinal ganglion cells. J Physiol. 1995; 486:207–221. [PubMed: 7562636]

Vecino E, Garcia-Grespo D, Garcia M, Martinez-Millan L, Sharma SC, Carrascal E. Rat retinal ganglion cells co-express brain derived neurotrophic factor (BDNF) and its receptor TrkB. Vision Res. 2002; 42:151–157. [PubMed: 11809469]

Villegas-Perez MP, Vidal-Sanz M, Bray GM, Aguayo AJ. Influences of peripheral nerve grafts on the survival and regrowth of axotomized retinal ganglion cells in adult rats. J Neurosci. 1988; 8:265–280. [PubMed: 2448429]

Wässle H, Boycott BB. Functional architecture of the mammalian retina. Physiol Rev. 1991; 71:447–480. [PubMed: 2006220]

Yang CY, Zhang J, Yazulla S. Differential synaptic organization of GABAergic bipolar cells and non-GABAergic (glutamatergic) bipolar cells in the tiger salamander retina. J Comp Neurol. 2003; 455:187–197. [PubMed: 12454984]

Zhang J, De Blas AL, Miralles CP, Yang CY. Localization of GABAA receptor subunits alpha 1, alpha 3, beta 1, beta 2/3, gamma 1, and gamma 2 in the salamander retina. J Comp Neurol. 2003; 459:440–453. [PubMed: 12687709]

Zhang J, Wang HH, Yang CY. Synaptic organization of GABAergic amacrine cells in the salamander retina. Vis Neurosci. 2004; 21:817–825. [PubMed: 15733337]

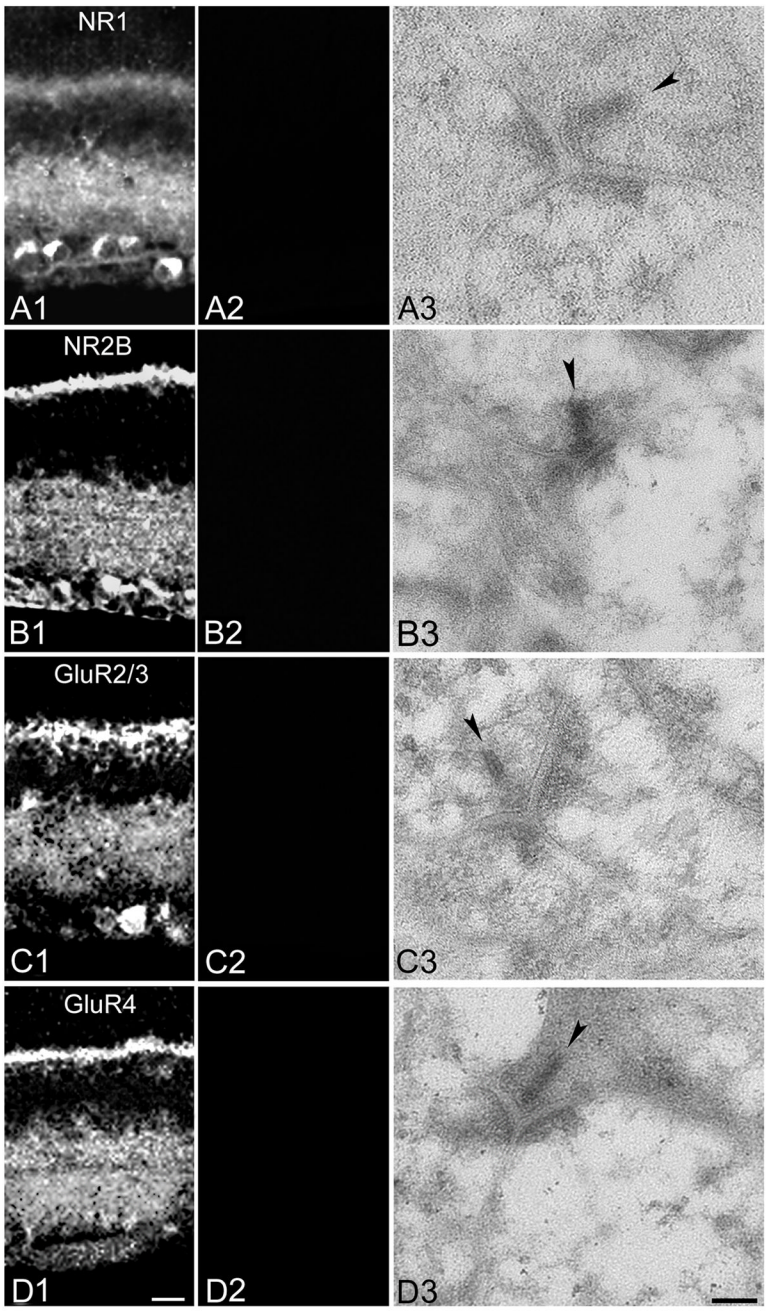

Figure 1. Preadsorption with antigen blocks primary antibody immunoreactivity

A: Images of retinal vertical sections showing anti-NR1 labeling pattern in control (A1) and following preadsorption of the antibody with the peptide antigen (A2). Panel A3 shows a representative EM section incubated with preadsorbed primary antibody. B: As in A, but with the anti-NR2B antibody. C: As in A, but with the anti-GluR2/3 antibody. D: As in A, but with the anti-GluR4 antibody. In EM images, presynaptic ribbons are indicated by arrowheads. Scale bars: 20 μm and 0.1 μm for light and electron micrographs, respectively.

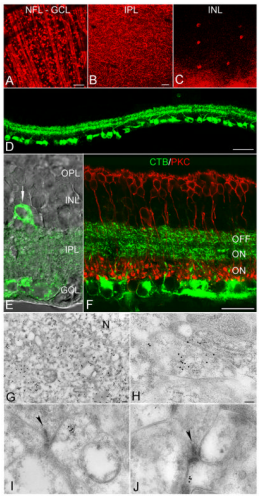

Figure 2. RGCs retrogradely labeled with CTB

A–C, Immunofluorescence images of flat-mounted retinas showing CTB-labeled RGCs in the nerve fiber layer (NFL), ganglion cell layer (GCL), and inner plexiform layer (IPL), as well as a small number of displaced RGCs in the inner nuclear layer (INL). D, Immunofluorescence image of transverse retinal sections showing CTB labeling at lower magnification. E, Superimposed immunofluorescence and differential interference contrast images showing CTB labeling in the IPL. Arrow indicates a displaced RGC. F, Co-labeling of CTB and PKC, a marker for rod bipolar cells, indicates that RGC dendrites ramify in the outer and middle thirds of the IPL, while rod bipolar cell terminals occupy the inner third. G, Electron micrograph showing that immunogold particles labeling CTB were excluded from the nucleus (N) of RGCs. H, A CTB-positive RGC dendrite in sublamina a. I and J, CTB-positive postsynaptic processes in sublamina a (I) and b (J). Presynaptic ribbons indicated by arrowheads. Scale bars: 50 μm (A–D), 20 μm (E, F) and 0.1 μm (G–J).

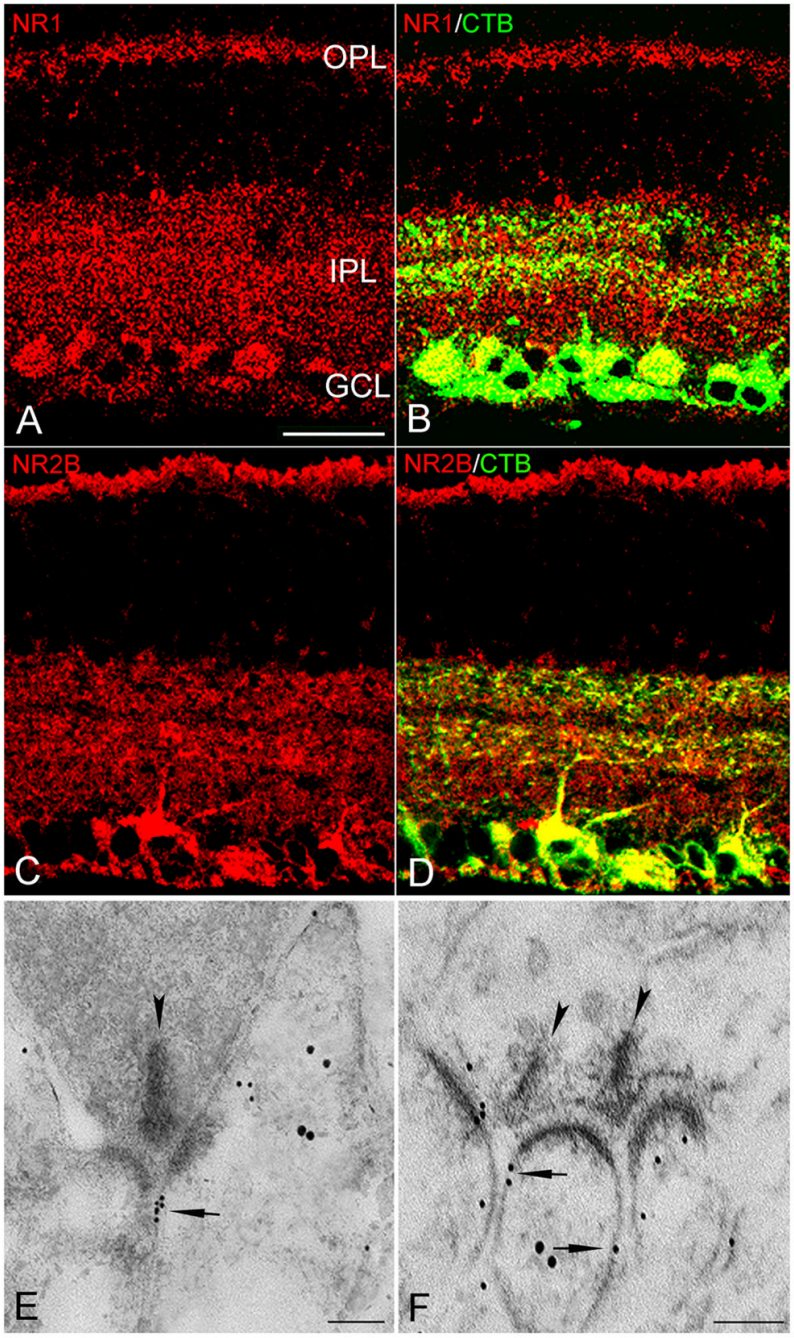

Figure 3. NMDAR immunoreactivity in the rat retina

A and C, NR1 and NR2B immunoreactivity in the IPL, OPL, as well somata in the GCL and INL. B and D, NR1- and NR2B-positive puncta colocalized with CTB-labeled RGC dendrites and somata (yellow). E and F, Electron micrographs showing double immunogold labeling of NMDARs (small particles) and CTB (large particles). At a cone dyad in the OFF sublamina, a cluster of small gold particles (arrow) in the extrasynaptic plasma membrane of RGC dendrites (E); at a dyad in the ON sublamina, two ribbons (arrowheads) each making a dyad with the same CTB-labeled RGC dendrite in which small gold particles (arrow) were on the extrasynaptic plasma membrane (F). Scale bar: 20 μm (A–D), 0.1 μm (E & F).

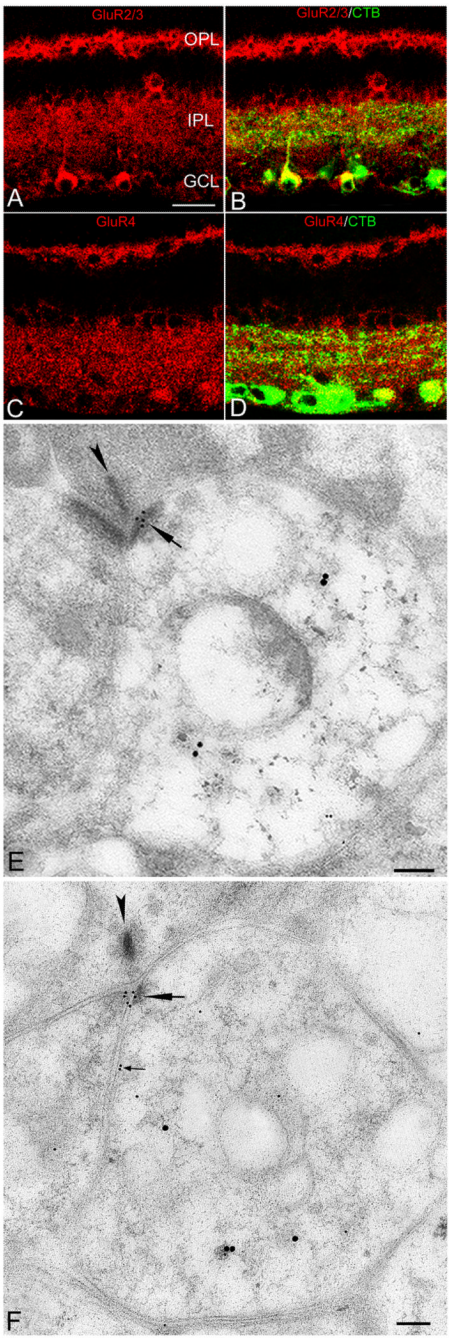

Figure 4. AMPAR immunoreactivity in the rat retina

A and C, GluR2/3 and GluR4 immunoreactivity in the IPL, OPL, and in somata within the GCL and INL. B and D, GluR2/3 - and GluR4 -positive puncta colocalized with CTB-labeled RGC dendrites and somata (yellow). E and F, Electron micrographs showing double immunogold labeling of AMPARs (small golds) and CTB (large golds) in the OFF and ON sublamina, respectively; small gold particles are clustered (large arrows) in the PSD of RGC processes. F, A rare example of an AMPA-positive RGC process expressing AMPARs perisynaptically (small arrows). Scale bar: 20 μm (A–D), 0.1 μm (E and F).

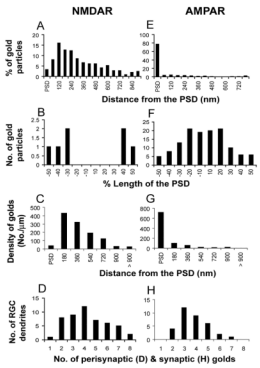

Figure 5. Quantitative comparison of NMDARs and AMPARs localization in RGC dendrites

A and E, Histograms show the tangential distribution of immunogolds for NMDARs (n=51, A) and AMPARs (n=48, E) within and outside the PSD. The perisynaptic region was divided into 60 nm bins. B and F, Histograms show the tangential distribution of immunogold particles labeling NMDARs (n=4 synapses, B) and AMPARs (n=48 synapses, F) within the PSD. C and G, Histograms show the density of immunogold particles labeling NMDARs (n=51, C) and AMPARs (n=48, G). The perisynaptic region was divided into 180 nm bins. D and H, Histograms showing the number of gold particles detected at NMDAR- and AMPAR-immunopositive synapses, respectively.

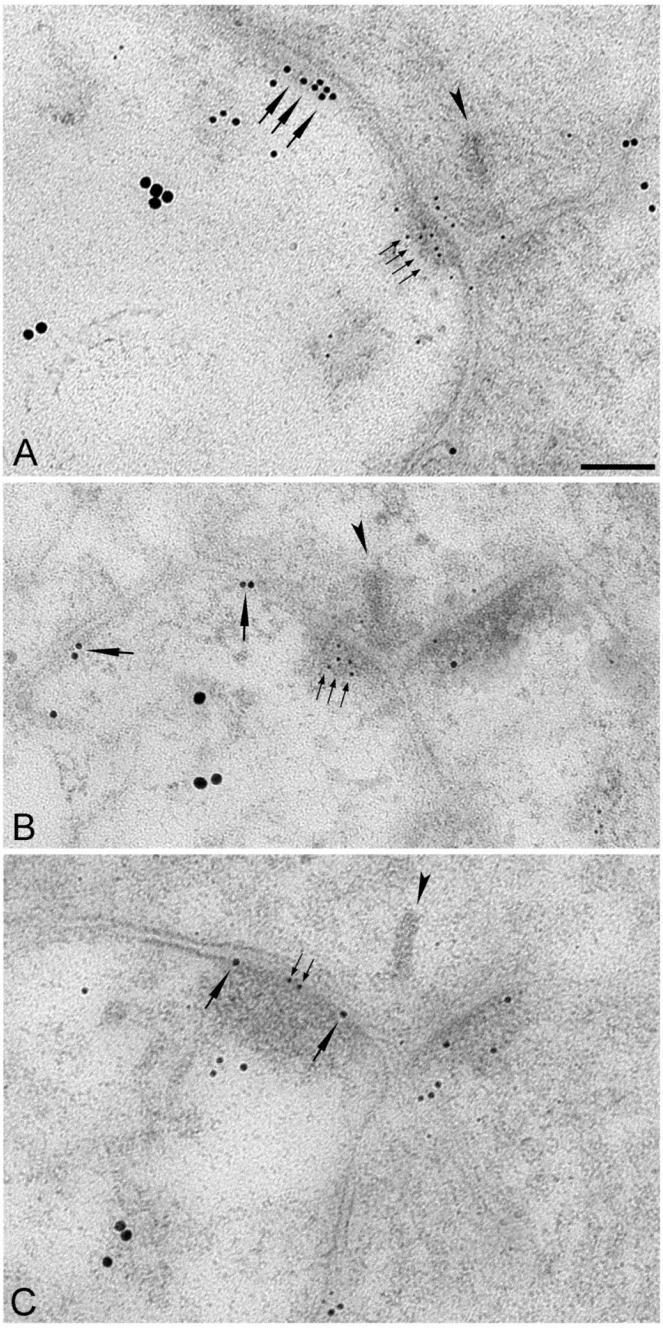

Figure 6. Simultaneous labeling of NMDARs, AMPARs and RGCs

Electron micrographs showing triple immunogold labeling of AMPARs (5 nm gold), NMDARs (10 nm gold) and CTB (18 nm gold). A and B, AMPAR gold particles (small arrows) were located in the PSD while NMDAR gold particles (large arrows) were perisynaptic on individual CTB-positive RGC dendrites in the ON and OFF sublamina, respectively. **(C)** A rare example of NMDARs and AMPARs co-localized within the PSD. Scale bar: 0.1 μm (A–C).

Table 1

Comparison of immunogold densities (Mean ± SE, gold/μm) of NMDARs and AMPARs in various cell membranes

LOCATION	NMDA	AMPA
I. The PSD of RGC	0.77 ± 0.38 (51)*	15.76 ± 1.78 (43)
II. Extrasynaptic membrane of RGC	2.98 ± 0.24 (51)	0.55 ± 0.15 (43)
III. Mitochondrial outer membrane	0.06 ± 0.02 (47)	0.08 ± 0.02 (43)
IV. Muller cell membrane	0.07 ± 0.02 (44)	0.11 ± 0.03 (43)
Ratios of signal to noise (*t* test)		
I/III	13**	197****
I/IV	11**	143****
II/III	50****	7***
II/IV	43****	5***

* The number of samples.

** P<0.1

*** P<0.005

**** P<0.0001 (Two-sided *t* test)